



Cite this: *Nanoscale*, 2022, **14**, 12129

# Pectin-assisted one-pot synthesis of MoS<sub>2</sub> nanocomposites for resistive switching memory application†

Honglei Wang,<sup>a</sup> Jun Shi,<sup>a</sup> Jingyu Zhang,<sup>a</sup> Zhehao Tao,<sup>a</sup> Hongguang Wang,<sup>\*b</sup> Qingqing Yang,<sup>a</sup> Peter A. van Aken<sup>b</sup> and Runfeng Chen <sup>\*a</sup>

Developing simple, large-scale, and environmentally-friendly ways to prepare two-dimensional (2D) semi-conductive hexagonal phase MoS<sub>2</sub> (2H-MoS<sub>2</sub>) nanocomposites remains a significant challenge. Herein, we propose a facile and green method for preparing few-layer MoS<sub>2</sub> nanosheets *via* a pectin-assisted one-pot synthesis (PAOS), where pectin serves as the surfactant and stabilizer to assist the direct exfoliation of bulk MoS<sub>2</sub> into few-layered semiconductive 2H-MoS<sub>2</sub> nanosheets in water, as well as a second functional part to produce the 2H-MoS<sub>2</sub>/pectin nanocomposites simultaneously. Based on the readily prepared 2H-MoS<sub>2</sub>/pectin nanocomposites, extraordinary flash memory devices with a typical bistable electrical switching and nonvolatile rewritable memory effect were realized, achieving a low threshold voltage below 2.0 V, a high ON/OFF ratio as high as  $5 \times 10^2$ , and a retention time longer than  $10^4$  s. Systematic investigations reveal that the electrical transition is due to the charge trapping and detrapping behaviors of the 2D 2H-MoS<sub>2</sub>/pectin nanocomposites. These findings through PAOS not only offer a general route for efficiently preparing 2H-MoS<sub>2</sub> nanosheets and nanocomposites, but also reveal the great potential of 2D MoS<sub>2</sub>-based materials in rectifying the electronic properties for high-performance memory devices.

Received 10th May 2022,  
Accepted 19th July 2022

DOI: 10.1039/d2nr02558b

rsc.li/nanoscale

## 1. Introduction

Two-dimensional (2D) layered materials are receiving considerable attention owing to their unique properties that are not present in bulk materials.<sup>1,2</sup> As the most representative transition metal dichalcogenide (TMD) material in 2D layers, molybdenum disulfide (MoS<sub>2</sub>) composed of covalently bonded S–Mo–S sheets interconnected by weak van der Waals forces has gained a lot of research interest because of its excellent optical and electrical characteristics originating from the various crystal structures and different electronic configurations.<sup>3,4</sup> Specifically, 2D MoS<sub>2</sub> in the hexagonal phase (2H-MoS<sub>2</sub>) analogous to that of graphene becomes semiconductive, providing obvious advantages in optoelectronic applications.<sup>5,6</sup> Moreover, the flat surface of MoS<sub>2</sub> nanosheets can be easily modified by covalent or non-covalent functionalization for

enhanced photonic,<sup>7</sup> electronic,<sup>8</sup> and catalytic properties<sup>9</sup> of 2D MoS<sub>2</sub> hybrid functional materials.

Nonvolatile memory devices based on 2D materials, which provide a chance to break the physical scaling limitations of data storage, have been a research focus over the past decades.<sup>10</sup> However, most methods for nanosheet preparation, such as chemical vapor deposition (CVD) and mechanical cleavage using Scotch tape, are difficult to be scaled up due to low yields and high costs.<sup>11</sup> Liquid phase exfoliation (LPE) in organic solvents such as *N*-methyl-2-pyrrolidone (NMP) with high surface tension ( $\sim 40$  mJ m<sup>−2</sup>) can prepare ultrathin MoS<sub>2</sub> nanosheets, but the relatively poor yield of nanosheets, use of high boiling-point and toxic solvents, and a long sonication time limit its further application.<sup>12</sup> Furthermore, MoS<sub>2</sub> nanosheets can act as a template to construct 2D nanocomposites through solution processing for high-performance nonvolatile memory devices.<sup>13</sup> Nevertheless, the preparation of MoS<sub>2</sub> nanocomposites is complicated, and it is also difficult to obtain ideal performance from the fabricated devices. Therefore, developing a large-scale, environmentally-friendly, and simple way to synthesize high-quality 2H-MoS<sub>2</sub> nanosheets and nanocomposites for high-performance nonvolatile memory devices remains a significant challenge.

<sup>a</sup>State Key Laboratory of Organic Electronics and Information Displays & Institute of Advanced Materials (IAM), Nanjing University of Posts & Telecommunications, 9 Wenyuan Road, Nanjing 210023, China. E-mail: iamrfchen@njupt.edu.cn

<sup>b</sup>Max Planck Institute for Solid State Research, Heisenbergstr. 1, 70569 Stuttgart, Germany. E-mail: hgwang@fkf.mpg.de

† Electronic supplementary information (ESI) available. See DOI: <https://doi.org/10.1039/d2nr02558b>



Herein, we present a method for efficiently fabricating 2H-MoS<sub>2</sub> nanosheets by pectin-assisted one-pot synthesis (PAOS) using only water as a solvent. Pectin functions as the surfactant and intercalant to efficiently promote the exfoliation process by expanding the interlayer during sonication. Moreover, pectin is adsorbed on the surface of 2H-MoS<sub>2</sub> nanosheets under non-covalent van der Waals forces to afford 2D 2H-MoS<sub>2</sub> nanocomposites in high concentrations ( $\sim 0.87 \text{ mg mL}^{-1}$ ). Table S1† summarizes the comparison of this work with several reported traditional LPE methods, showing that the proposed PAOS is rather facile, convenient, and environmentally friendly. The facilely prepared 2D 2H-MoS<sub>2</sub> nanocomposites in one pot can be used as the active layer of the memory device directly, which exhibits advanced performances with a low threshold voltage below 2.0 V, a high ON/OFF ratio as high as  $5 \times 10^2$ , and a retention time longer than  $10^4 \text{ s}$  in extraordinary nonvolatile flash memory devices. These performances outperform those of most MoS<sub>2</sub>-based memory devices (Table S2†) and will further push forward the fundamental research of 2D hybrid materials in advanced nanoelectronic applications.

## 2. Experiment

### 2.1 Preparation of 2H-MoS<sub>2</sub>/pectin nanocomposites

Typically, 30 mL deionized (DI) water was mixed with the desired amount of pectin powder (30, 60, 150, or 300 mg) in a glass bottle. When the pectin was completely dissolved, 300 mg bulk MoS<sub>2</sub> was added to the pectin solution. Then, the mixture was probe sonicated in an ultrasonic bath for various times from 0.5 to 5.0 h (ultrasonic with temperature controller, GEX 500). The resultant dispersions were centrifuged for 30 min at 2000 rpm to remove the bulk MoS<sub>2</sub> that has not been exfoliated. Next, the dispersions were centrifuged for 30 min at 5000 rpm to collect the precipitate of 2H-MoS<sub>2</sub>/pectin nanocomposites. The two-step centrifugation ensures that all of the bulk powder and dissolved species are removed. The obtained 2H-MoS<sub>2</sub>/pectin nanocomposites in one pot were named MP<sub>x</sub>, where  $x$  is their weight ratio (MoS<sub>2</sub> : pectin =  $x$  : 1).

### 2.2 Fabrication and measurement of the diode memory devices

The memory devices were made with a diode device structure comprising 2H-MoS<sub>2</sub>/pectin hybrid nanocomposites sandwiched between an indium-tin-oxide (ITO) bottom electrode and an aluminum (Al) top electrode.<sup>14</sup> The patterned ITO glass substrates were first cleaned with detergent, alcohol, acetone and DI water followed by drying for 2 h in a vacuum oven at 120 °C and UV-zone treatment for 15 min. To remove the residual solvents, the 2H-MoS<sub>2</sub>/pectin nanocomposites dispersed in DI water were spin-coated onto the ITO surface and annealed at 100 °C for 15 min. The spin-coating conditions were optimized to alter the film thickness, which was then measured using a profilometer (Dektak XT). Finally, an Al electrode with a thickness of 100 nm was thermally evaporated

onto the film surface through a shadow mask under a system pressure of  $5 \times 10^{-4} \text{ Pa}$ . The device had an active area of  $0.4 \times 0.4 \text{ mm}^2$ , and the current-voltage ( $I$ - $V$ ) characteristics of the devices were determined using a Keithley 2400 source-measure unit.

## 3. Results and discussion

The method of PAOS developed for the preparation of 2H-MoS<sub>2</sub>/pectin nanocomposites is schematically shown in Fig. 1a. Briefly, the commercial MoS<sub>2</sub> powder (Fig. 1b) was probe sonicated in DI water in the presence of pectin powder (Fig. 1c). Pectin contains both the hydrophobic ester and hydrophilic carboxyl groups; the hydrophobic part allows the molecule to adsorb onto the surface of the MoS<sub>2</sub> nanosheets and the hydrophilic component allows the interaction with water stabilizing the materials. Therefore, pectin dissolved in water serves as both surfactant and intercalant to exfoliate MoS<sub>2</sub> into nanosheets and disperse them in water. The resulting mixture was centrifugated, collected and dispersed to obtain the dark green dispersions of 2H-MoS<sub>2</sub>/pectin nanocomposites in different solvents. An obvious Tyndall effect of the dispersions was observed (Fig. 1a, inset), suggesting the successful exfoliation of the bulk material. Furthermore, these suspensions were highly stable under ambient conditions, and no obvious precipitation could be observed after 2 months.

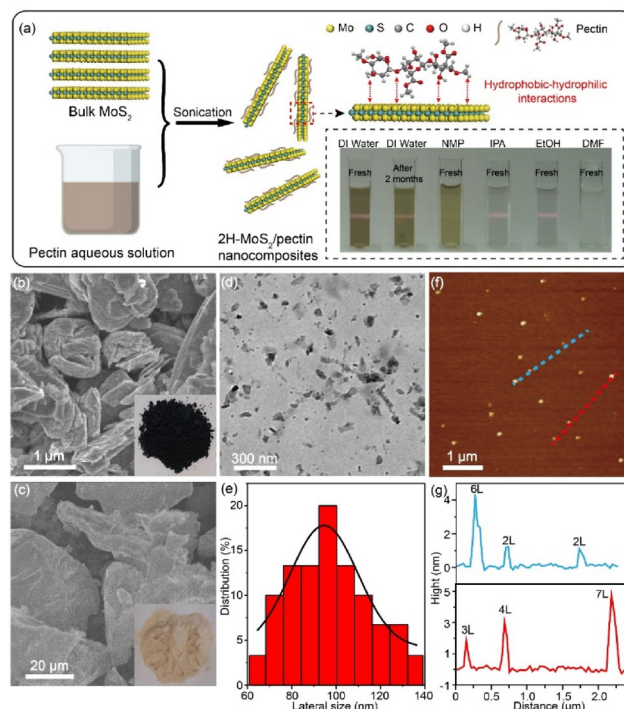


**Fig. 1** 2H-MoS<sub>2</sub>/pectin nanocomposites prepared by PAOS. (a) Preparation scheme and the Tyndall effect in various solvents (inset). (b) and (c) SEM images and photographs (inset) of (b) bulk MoS<sub>2</sub> and (c) pectin powder. (d) TEM image, (e) lateral size distributions, (f) AFM image and (g) height profiles of the MoS<sub>2</sub> nanosheets of MP10.



Among the different solvents of NMP, isopropanol (IPA), ethanol (EtOH), and *N,N*-dimethylformamide (DMF), DI water has the highest preparation efficiency. The high solubility (MP10, 0.87 mg mL<sup>-1</sup>) of 2H-MoS<sub>2</sub>/pectin nanocomposites in water is extremely desirable for device fabrication *via* solution processing, mainly because water is a low-boiling solvent and is environmentally-friendly and can evaporate quickly during film deposition. 2H-MoS<sub>2</sub> nanosheets without the pectin content could be further prepared by repeating the washing and centrifugation five times, followed by redispersing in water.

The microstructure and surface morphology of the nanocomposites prepared by the PAOS method was investigated using transmission electron microscopy (TEM) and atomic force microscopy (AFM). The TEM images at different magnifications (Fig. 1d) verify the presence of nanocomposites in MP10 with the lateral size distribution in the range of 90–110 nm (Fig. 1e). TEM (Fig. S1†) and AFM (Fig. 1f) images of the PAOS-prepared MoS<sub>2</sub> nanosheets further confirmed the success of the exfoliation and the corresponding height profile (Fig. 1g) shows that the thickness of most MoS<sub>2</sub> nanosheets is less than 5 nm. Considering that the thickness of a single layer of 2H-MoS<sub>2</sub> is about 0.65–0.70 nm,<sup>15</sup> the prepared MoS<sub>2</sub> nanosheets are mainly composed of 1–7 layers.

Furthermore, the crystal structure and lattice parameters of the prepared MoS<sub>2</sub> nanosheets were characterized by atomically resolved scanning transmission electron microscopy (STEM) investigations (Fig. 2a). Individual Mo and S atoms forming hexagonal configurations could be clearly resolved. The measured lattice distance is about ~0.27 nm, which is consistent with the value from a high-resolution TEM image (Fig. S2†), corresponding to the reported lattice spacing *d*(1100) of MoS<sub>2</sub> [ICSD no. 84180].<sup>16</sup> The selected area electron diffraction (SAED) pattern (Fig. S2†) exhibits the typical six-fold symmetry of 2H-MoS<sub>2</sub>, indicating that the hexagonal structure of the nanosheets received little damage during the PAOS

treatment. The high-angle annular dark-field STEM (HAADF-STEM) image of MP10 shows that these prepared MoS<sub>2</sub> nanosheets have a typical terraced structure with a few steps for a few layers of 2H-MoS<sub>2</sub> (Fig. 2b). The electron energy-loss spectroscopy (EELS) spectrum demonstrates the presence of Mo, S, C, and O in MP10 (Fig. S3†). Their corresponding elemental maps indicate that pectin was mostly adsorbed on the surface of MoS<sub>2</sub> nanosheets, further demonstrating that we have successfully prepared 2H-MoS<sub>2</sub>/pectin nanocomposites (Fig. 2c).

Compared with pure MoS<sub>2</sub>, pectin doping led to a smaller contact angle of water and thus better wettability (Fig. 3a), which can minimize the exfoliation energy and stabilize the exfoliated MoS<sub>2</sub> nanosheets. Also, it is beneficial for the formation of high-quality films for the fabrication of semiconductor devices. We suspect that the bulk MoS<sub>2</sub> particles are fragmented, while the water-soluble pectin is uniformly adsorbed on the surface of MoS<sub>2</sub> in the nanocomposites for the facile MoS<sub>2</sub> exfoliation and good wettability. The photo-physical properties of the facilely prepared 2H-MoS<sub>2</sub> nanosheets were investigated using UV-vis absorption spectroscopy (Fig. 3b and c). The intrinsic peaks at 616 and 676 nm are attributed to the characteristic A1 and B1 direct excitonic transitions of 2H-MoS<sub>2</sub>. Because these two absorption peaks are closely related to the concentrations of 2H-MoS<sub>2</sub> nanosheets in the Lambert–Beer law, the absorbance strength was used to quantitatively characterize the efficiency of LPE.<sup>17</sup> At the elongated sonication time, the exfoliation efficiency of the samples (the weight ratio of MoS<sub>2</sub> and pectin powder was 10 : 1) was improved with an enhanced absorbance strength (Fig. 3b), but a prolonged time over 3.0 h seems to be unnecessary. During the sonication, pectin acts as a surfactant so that it can be adsorbed on the surface of MoS<sub>2</sub> to improve the exfoliation efficiency. As the concentration of pectin solution increased from MP10 to MP1, the yield of nanosheets increased dramatically, and the final concentrations of MP1 and MP10 dispersions reached 2.26 and 0.87 mg mL<sup>-1</sup>, respectively. Impressively, the nanocomposite dispersions were very stable and only a little sedimentation could be observed over months. To understand the excellent aqueous stability, the zeta potentials of the pure pectin and 2H-MoS<sub>2</sub>/pectin aqueous dispersions were measured. The dispersed pectin, fresh MP10, and MP10 after 2 months were all negatively charged with a zeta potential of –30.5 mV, –14.1 mV, and –12.5 mV, respectively (Fig. 3c). The values well exceeded the accepted value for a stable colloid, showing that the highly aqueous stable pectin greatly improves the aqueous stability of its nanocomposites.<sup>18</sup>

Furthermore, Raman spectroscopy was used to probe the transformation of bulk powders of MoS<sub>2</sub> into 2D few-layered structures. From the two characteristic E<sub>2g</sub><sup>1</sup> (in-plane bending) and A<sub>1g</sub> (stretching of sulfur atoms) vibrations located around 383.6 and 408 cm<sup>-1</sup>, obvious shifts in the positions of these peaks in comparison with those of pristine bulk MoS<sub>2</sub> demonstrated the good exfoliation of the bulk powders to the few-layered nanosheets (Fig. 3e).<sup>19</sup> X-ray diffraction (XRD) patterns

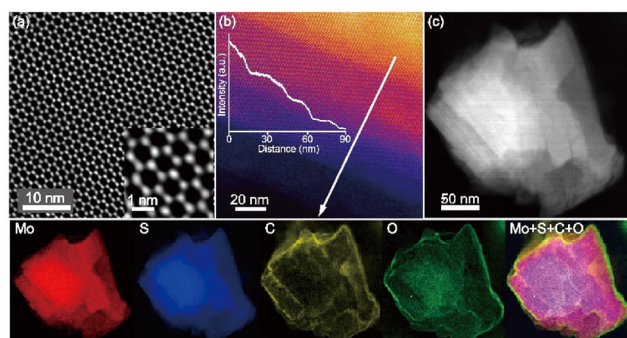


**Fig. 2** Structure and elemental distribution of the 2H-MoS<sub>2</sub>/pectin nanocomposites. (a) Atomically resolved STEM image, where individual Mo and S atoms form the hexagonal structure (inset). (b) HAADF-STEM image and the corresponding intensity profile (inset). (c) The HAADF-STEM image and STEM-EELS maps of Mo (red), S (blue), C (yellow), and O (green), and the reconstructed composite image (Mo + S + C + O).





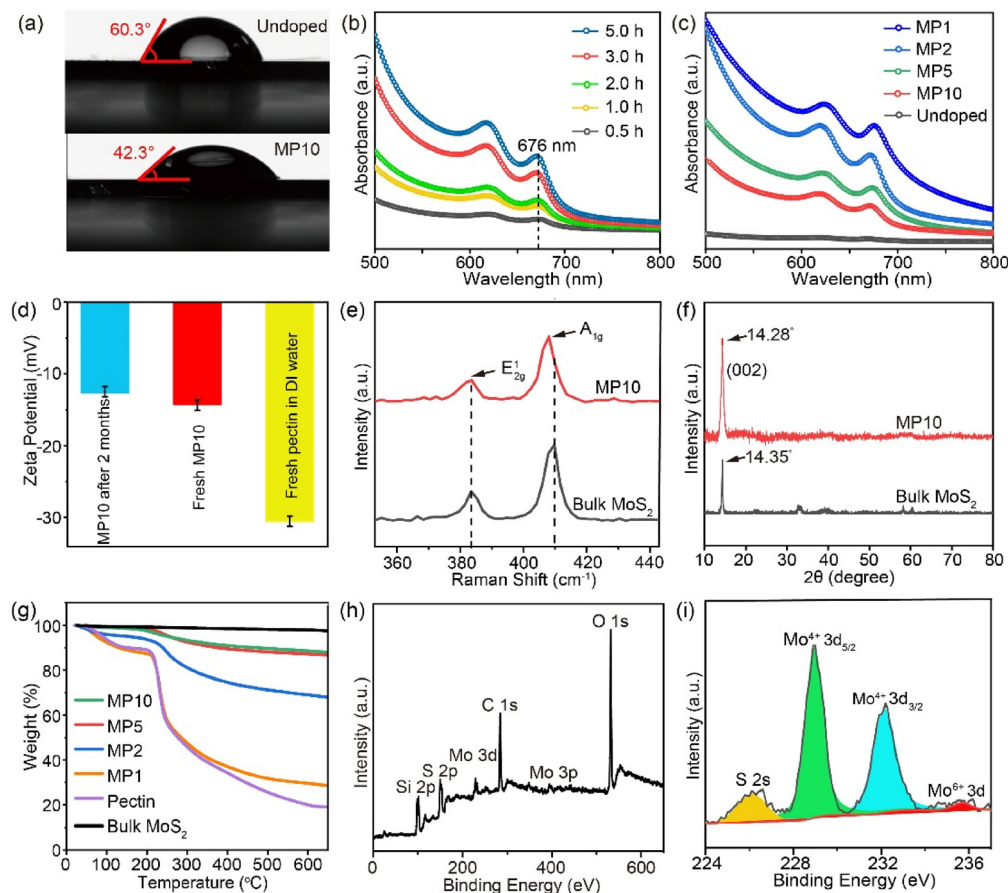


**Fig. 3** Properties of the 2H-MoS<sub>2</sub>/pectin nanocomposites. (a) Contact angles of the pure MoS<sub>2</sub> nanosheet (undoped) and MP10 with DI water. (b and c) UV-vis absorption spectra of the MoS<sub>2</sub>/pectin nanocomposites prepared with (b) different sonication times from 0.5 to 5.0 h at a pectin doping ratio of 10 wt% and (c) different weight doping ratios of pectin with 2.0 h of sonication. (d) Zeta potential of fresh MP10, MP10 after 2 months, and pure pectin dispersions. (e and f) Raman spectra and XRD patterns of bulk MoS<sub>2</sub> and MP10. (g) TGA curves of the bulk MoS<sub>2</sub> and MoS<sub>2</sub> nanocomposites with different contents of pectin. (h and i) XPS and high-resolution XPS spectra of MP10.

(Fig. 3f) show that bulk MoS<sub>2</sub> has many strong and sharp peaks in the range from 10 to 80°, matching with the hexagonal 2H-MoS<sub>2</sub> (JCPDS: 65-1951). Nevertheless, the peak of the (002) reflection was broadened and shifted (14.35° in bulk MoS<sub>2</sub>, and shift to 14.28°) in nanocomposites, indicating that the introduction of pectin increased the interlayer spacing of bulk MoS<sub>2</sub>.<sup>20</sup>

The actual contents of MP10, MP5, MP2, and MP1 were measured by thermogravimetric analysis (TGA) tests (Fig. 3g). At high temperatures over 600 °C, all the organic components could be largely (80 wt%) removed, but the inorganic MoS<sub>2</sub> remained almost unchanged. Therefore, the contents of pectin in the nanocomposites could be determined, which are 12%, 13.6%, 38% and 88% in MP10, MP5, MP2 and MP1, respectively.<sup>21</sup> Obviously, the actual contents of pectin are even slightly larger than the initial feed ratios owing to the strong interactions between pectin and the MoS<sub>2</sub> nanosheet in forming stable nanocomposites. The chemical states of the nanocomposites were investigated by X-ray photoelectron spectroscopy (XPS; Fig. 3h and i). Two distinct peaks at 229.0 eV and 232.2 eV corresponding to the Mo<sup>4+</sup> 3d<sub>5/2</sub> and Mo<sup>4+</sup> 3d<sub>3/2</sub>

excitation of the hexagonal 2H-MoS<sub>2</sub> phase almost without signals of the 1T phase were clearly observed.<sup>22</sup> Compared to the previous reports regarding LPE and alkali ion intercalations with a significant Mo<sup>6+</sup> peak at 235.4 eV from MoO<sub>3</sub>, this peak could be hardly observed in the XPS result of the MoS<sub>2</sub> nanosheets prepared by our PAOS method, which suggests that our process effectively prevents the oxidation of the nanosheets.<sup>23</sup> A weak peak at 235.6 eV suggests a trace of oxidized Mo (Mo<sup>6+</sup> 3d), possibly originating from the partial oxidation of Mo atoms at the edges or defects of MoS<sub>2</sub> sheets.

In an effort to explore the application potential of the newly constructed and facily prepared stable, water-dispersible, and 2D 2H-MoS<sub>2</sub> nanocomposites, MP10 was tested as active layers in direct charge transport diode devices with a configuration of ITO/MP10(25 nm)/Al, where ITO and Al are the bottom and top electrodes, respectively (Fig. 4). The AFM image revealed that the root-mean-square roughness (RMS) of the MP10 film was 1.73 nm, indicating a good film forming property with high uniformity of the 2D nanocomposites (Fig. S4†). Excitingly, an extraordinary flash memory behavior was identified from the characteristic *I*-*V* curves of the fabricated



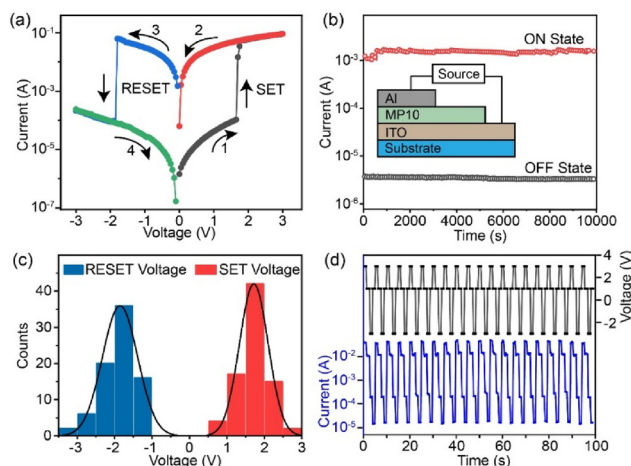


**Fig. 4** Diode memory device based on MP10. (a)  $I$ - $V$  characteristics of the ITO/MP10/Al diode memory device. (b) Retention times of the ON and OFF states of the memory device probed with a voltage of 0.1 V. Inset: memory device configuration. (c) Statistics histograms of SET/RESET voltages. (d) Write-read-erase-read (WRER) cycles of the memory device. Voltages for WRER cycles are +3, 1, -3, and 1 V, respectively.

2H-MoS<sub>2</sub>/pectin-based diode measured at room temperature and under an ambient atmosphere (Fig. 4a).<sup>15</sup> The device was initially OFF with a low current density, and when a positive voltage was applied from 0 to 3 V (first sweep), a rapid current jump occurred at 1.6 V to establish an ON state, representing a “writing” process in the memory device. The high conductivity could be read in the subsequent positive sweep (second sweep) and reverse sweep (third sweep). Importantly, when the negative sweep voltage was less than -1.8 V, the high-conductive ON state could be switched back to the original low-conductive OFF state, serving as the “erasing” process of the memory device; the OFF state could be read (fourth sweep) and reprogrammed to an ON state in the next positive sweep, resulting in a repeatable “write-read-erase-read-rewrite” cycle for a rewritable nonvolatile flash memory device. Moreover, the memory device was highly stable with a threshold voltage below 2.0 V and an ON/OFF current ratio over  $5 \times 10^2$ , and a retention time longer than  $10^4$  s (Fig. 4b). As shown in Fig. 4c, we also tested the uniformity of the switching voltage distribution in 8 randomly selected device cells. The averaged SET voltage and RESET voltage values were 1.7 V and -2 V, respectively. The difference between SET and RESET voltages was significant enough to guarantee reading reliability. The flash memory based on MP10 had great repeatability, allowing for good performance control in practical applications. The device is favorable for the steady running of flash type memory writing-reading-erasing cycles acting on continuous voltage signals at 3 V (write), 1 V (read), -3 V (erase), and 1 V (read), respectively, affording over 20 cycles of write-read-erase-read (WRER) in 100 s (Fig. 4d). The stable and high ON/OFF current ratio of the flash memory based on MP10 is promising and advantageous to minimize the misreading probability for the

long-term operation of memory devices (Table S2†). Meanwhile, we fabricated memory devices with other contents of pectin in 2H-MoS<sub>2</sub>/pectin nanocomposites, as shown in Fig. S5.† While increasing the content of pectin, the device exhibited the storage characteristics of write-once read-many-times (WORM) (Fig. S5b†). On continuing to increase the content of pectin, the storage phenomenon would disappear (Fig. S5c†), indicating that both organic and inorganic components of the nanocomposites contribute to the electric rectification and their ratios are crucial in modulating the memory device performance.

In order to understand the conductance switching mechanism of the flash memory device, the experimental  $I$ - $V$  curves were studied by model fitting. Four distinct regions were observed in the  $I$ - $V$  plot and four different conduction mechanisms in each region were identified (Fig. 5a). In the OFF state, the plot of  $\ln(I)$  versus  $V^{1/2}$  from 0 to 0.8 V (region A) was fitted to a straight line (Fig. 5b). The linear characteristic indicated that the conduction process was probably due to a thermionic emission, and the charge injection dominated the conduction mechanism.<sup>24</sup> In region B, the plot of  $\ln(I)$  versus  $\ln(V)$  over the voltage sweep from 0.8 V to 1.65 V (Fig. 5c) revealed a linear relationship with a slope of 1.75 (nearly 2) (Fig. 5c), indicating that a space-charge limited current (SCLC) dominates the carrier transport process.<sup>25</sup> In the switching region (region C), as the voltage is increased, the current increases exponentially as  $I \sim V^m$  ( $m = 23.7$ ) (Fig. 5c). The plot of  $\ln(I)$  versus  $\ln(V)$  obeys Ohm's law in region D with a slope of 1.0, when the voltage reaches the switching threshold (Fig. 5d), demonstrating that ohmic conduction dominates in the memory device.<sup>24</sup>

Based on the results and discussions mentioned above, we propose that the charge trapping and detrapping behaviors of MoS<sub>2</sub> in the pectin matrix are responsible for the electronic transition of 2D nanocomposites. The large barrier causes low

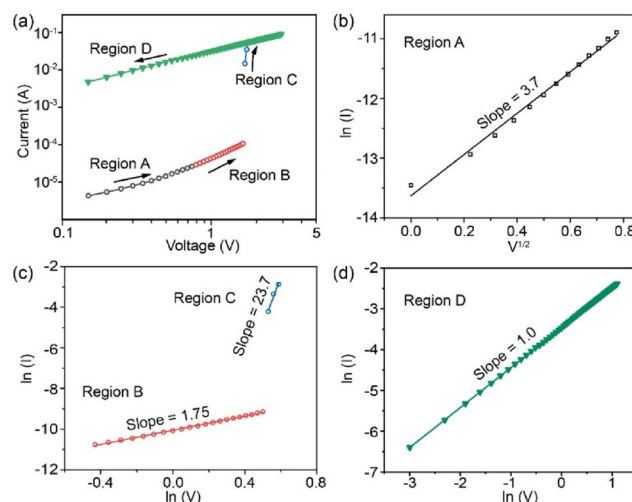


**Fig. 5** Experimental  $I$ - $V$  characteristics of the flash memory device at the positive voltage sweep with fitted lines of  $I$ - $V$  curves (a) in regions A (b), B (c), C (c), and D (d).

injection efficiency at low voltage, resulting in thermionic emission in the OFF state. The thermionic process across the electron-injection or hole-injection barrier injects carriers into the pectin dielectric at higher voltages. The charge was transferred from pectin to MoS<sub>2</sub>, which was subsequently trapped by MoS<sub>2</sub> due to its lower energy level and quantum confinement effect, as well as a lower free carrier density than the trap density caused by MoS<sub>2</sub>, resulting in the SCLC model.<sup>26,27</sup> The injected carriers increased greatly as the bias exceeded the switching voltage, leading to the rapid current change. After this transition, almost all the traps were occupied by charges. As a result, the device exhibited the ohmic behavior in the ON state. When a reverse voltage was applied, the trapped charges would be detrapped. The internal electrical field induced by the trapped charges disappeared. Therefore, the device returned to its initial high resistance state, and the erasing process of data storage was completed.

## 4. Conclusions

In summary, an efficient PAOS method was developed to prepare high-quality 2D 2H-MoS<sub>2</sub>/pectin nanocomposites for optoelectronic devices. This method has the advantages of facileness, high efficiency, and environmental friendliness, where pectin serves as a surfactant and stabilizer to assist the direct exfoliation of bulk MoS<sub>2</sub> in water to prepare few-layered MoS<sub>2</sub> based nanosheets and nanocomposites. An extraordinary flash memory device with a characteristic bistable electrical switching and nonvolatile rewritable memory effect was obtained based on the synthesized 2H-MoS<sub>2</sub>/pectin nanocomposites, exhibiting a low threshold voltage below 2.0 V, a high ON/OFF ratio of  $5 \times 10^2$ , and a retention period longer than  $10^4$  s. The electrical transition of the device might be attributed to the charge trapping and detrapping behaviors of the MoS<sub>2</sub> nanosheet in the pectin matrix under an electrical field. These results *via* PAOS should provide important hints for the efficient and green preparation of 2D nanocomposites, which are highly attractive for semiconductor device applications.

## Author contributions

H. Wang prepared the samples and wrote the manuscript. J. Shi prepared the samples and devices. H. Wang, P. A. van Aken, and R. Chen designed and conceived this work. J. Zhang, Z. Tao, Q. Yang, and H. Wang contributed to measurements. H. Wang and R. Chen wrote the manuscript. H. Wang, P. A. van Aken, and R. Chen discussed some questions and modified the manuscript. R. Chen guided this project.

## Conflicts of interest

There are no conflicts to declare.

## Acknowledgements

This study was supported in part by the National Natural Science Foundation of China (61875090, 21772095 and 91833306), the Fifth 333 Project of Jiangsu Province of China (BRA2019080), the Key Giant Project of Jiangsu Educational Committee (19KJA180005), the 1311 Talents Program of Nanjing University of Posts and Telecommunications (Dingshan and innovative team), and the European Union's Horizon 2020 Research and Innovation Programme (no. 823717 – ESTEEM3).

## References

- 1 K. M. Wyss, D. X. Luong and J. M. Tour, *Adv. Mater.*, 2022, 2106970.
- 2 Y. Dong, Y. Xu, W. Li, M. Wu, E. Manske, J. Kroeger and Y. Lei, *Small*, 2019, 15, 1900497.
- 3 K. Yao, Z. Xu, M. Ma, J. Li, F. Lu and J. Huang, *Adv. Funct. Mater.*, 2020, 30, 2001484.
- 4 Y. Duan, Y. Liu, Z. Chen, D. Liu, E. Yu, X. Zhang, H. Fu, J. Fu, J. Zhang and H. Du, *Green Chem.*, 2020, 22, 44–53.
- 5 H. Peng, D. Wang and S. Fu, *Composites, Part B*, 2021, 108742.
- 6 Y. Dong, C. Yan, H. Zhao and Y. Lei, *Small Struct.*, 2022, 2100221.
- 7 Z. Hu, Z. Wu, C. Han, J. He, Z. Ni and W. Chen, *Chem. Soc. Rev.*, 2018, 47, 3100–3128.
- 8 J. H. Han, M. Kwak, Y. Kim and J. Cheon, *Chem. Rev.*, 2018, 118, 6151–6188.
- 9 H. Wang, C. Li, P. Fang, Z. Zhang and J. Z. Zhang, *Chem. Soc. Rev.*, 2018, 47, 6101–6127.
- 10 Y. Lei, R. Cheng, Y. Wen, C. Liu and J. He, *Adv. Mater.*, 2021, 33, 2007081.
- 11 J. Zheng, H. Zhang, S. Dong, Y. Liu, C. T. Nai, H. S. Shin, H. Y. Jeong, B. Liu and K. P. Loh, *Nat. Commun.*, 2014, 5, 2995.
- 12 C. X. Hu, Y. Shin, O. Read and C. Cinzia, *Nanoscale*, 2021, 13, 460–484.
- 13 H. Wang, P. Cheng, J. Shi, D. Wang, H. Wang, J. Pezoldt, M. Stich, R. Chen, P. A. van Aken, W. Huang and P. Schaaf, *Green Chem.*, 2021, 23, 3642–3648.
- 14 R. Chen, C. Lin, H. Yu, Y. Tang, C. Song, L. Yuwen, H. Li, X. Xie, L. Wang and W. Huang, *Chem. Mater.*, 2016, 28, 4300–4306.
- 15 W. Lv, H. Wang, L. Jia, X. Tang, C. Lin, L. Yuwen, L. Wang, W. Huang and R. Chen, *ACS Appl. Mater. Interfaces*, 2018, 10, 6552–6559.
- 16 H. Wang, J. Niu, J. Shi, W. Lv, H. Wang, P. A. van Aken, Z. Zhang, R. Chen and W. Huang, *Small*, 2021, 17, 2102263.
- 17 H. Sim, J. Lee, B. Park, S. J. Kim, S. Kang, W. Ryu and S. C. Jun, *Nano Res.*, 2016, 9, 1709–1722.
- 18 L. Lei and Y. Zhang, *Composites, Part B*, 2021, 109077.



- 19 H. Wang, W. Lv, J. Shi, H. Wang, D. Wang, L. Jin, J. Chao, P. A. van Aken, R. Chen and W. Huang, *ACS Sustainable Chem. Eng.*, 2019, **8**, 84–90.
- 20 X. Wang and P. Wu, *ACS Appl. Mater. Interfaces*, 2018, **10**, 2504–2514.
- 21 Y. Li, H. Zhu, F. Shen, J. Wan, S. Lacey, Z. Fang, H. Dai and L. Hu, *Nano Energy*, 2015, **13**, 346–354.
- 22 A. Jawaid, D. Nepal, K. Park, M. Jespersen, A. Qualley, P. Mirau, L. F. Drummy and R. A. Vaia, *Chem. Mater.*, 2015, **28**, 337–348.
- 23 G. Eda, H. Yamaguchi, D. Voiry, T. Fujita, M. Chen and M. Chhowalla, *Nano Lett.*, 2011, **11**, 5111–5116.
- 24 J. Liu, Z. Zeng, X. Cao, G. Lu, L. Wang, Q. Fan, W. Huang and H. Zhang, *Small*, 2012, **8**, 3517–3522.
- 25 M. A. Lampert and P. Mark, *Current Injection in Solids*, New York, 1970.
- 26 A. Kuc, N. Zibouche and T. Heine, *Phys. Rev. B: Condens. Matter Mater. Phys.*, 2011, **83**, 245213.
- 27 M. Y. Ni, H. L. Wang, L. X. Chen, C. Q. Sheng, X. Peng, K. Deng, C. M. Wang, R. F. Chen, Q. D. Zeng and J. H. Wan, *Appl. Surf. Sci.*, 2021, **537**, 147313.

